ISTITUTO NAZIONALE DI FISICA NUCLEARE

Sezione di: Roma1 - LNF

SPARC/LS-06/002
20 Febbraio 2006

UV-IR
Cross Correlator

Massimo Petrarca[1], C. Vicario[2], S. Cialdi[3], P. Musumeci[1], G. Gatti[2], A. Ghigo[2], M. Mattioli[1]
[1)] *INFN, Sez. of Roma1, Dip. Scienze Fisiche, Univ. of Rome: "La Sapienza"*
[2)] *INFN, Laboratori Nazionali di Frascati (LNF)*
[3)] *INFN, Sez. of Milan*

Abstract

We report on the technique adopted to measure with a high resolution ($\sim 300fs$), the UV time distribution of the SPARC photoinjector laser pulses in the range $200fs$ to $12ps$. The theory of a scanning cross correlator based on difference frequency generation process in a BBO crystal is briefly reviewed. The realization of a prototype is discussed and a few measurements about the effects of the beam alignement and spot size due to the spatial chirp of the UV beam, are reported.

PACS:42.79.-e,07.60.-j;42.65.-Re,42.65.-k

Published by Laboratori Nazionali di Frascati

1 Introduction

Nowadays, UV laser pulses are commonly produced for many purposes; we refer in the following to the SPARC laser photoinjector [1–4]. In this project [1], UV pulses with uniform temporal profile, rise and fall time less than $1ps$ and uniform spatial distribution are required to drive a high-brilliance rf linac photo-injector [5,6]. The photo-injector itself is used to drive a high-brightness Self Amplified Spontaneous Emission Free Electron Laser (SASE-FEL) in the visible and soft X-rays region.

It is extremely important to know all the parameters which characterize the UV laser pulse: the spectral amplitude, the temporal shape (intensity profile) and the phase. Usually to measure UV pulse time distribution, a streak camera is used. The drawback of this system is to be expensive for the low resolution type ($\sim> 2ps$), and much expensive for the high resolution models ($\sim 350fs$). Because of this reason, we developed an optical diagnostic device, which has an affordable price compare to the hundred thousand euros necessary to buy a streak camera.

The main optical techniques adopted to measure the temporal pulse characteristics use the 2^{nd} and 3^{rd} order autocorrelation or cross-correlation functions [7] [8] [9]. Both this techniques are based on a non-linear interaction of the same beam (autocorrelation) or of two different beams (cross-correlation) inside a non linear crystal.

In general [7], an intensity correlation function is defined as:

$$A(\tau) = \int_{-\infty}^{\infty} I_1(t) I_2(t-\tau) dt \tag{1}$$

where I_1, I_2 are the intensities of the two beams entering into the crystal; I_2 is usually called: "the reference pulse" or the "scanning pulse" and it is delayed of a time τ with respect to the first beam's pulses that we want to analyze.

When the two intensity profiles in Eq. (1) are the same but for the time delay between them (that is: $I_1 = I_2 = I$); Eq. (1) gives:

$$A_2(\tau) = \int_{-\infty}^{\infty} I(t) I(t-\tau) dt \tag{2}$$

which is called a "second order autocorrelation function".

In general it is called "autocorrelation function" of order $(n+1)$ the following function:

$$A_n(\tau) = \int_{-\infty}^{\infty} I(t) I^n(t-\tau) dt \tag{3}$$

For $n = 2$ Eq. (3) gives a third order autocorrelation function:

$$A_3(\tau) = \int_{-\infty}^{\infty} I(t) \cdot I^2(t-\tau) dt \tag{4}$$

Substituting $t - \tau = y$, Eq (2) can also be written (that holds only for the second order correlation function):

$$A_2(\tau) = \int_{-\infty}^{\infty} I(y+\tau) \cdot I(y) dy \tag{5}$$

As it is shown in Eq. (2), the 2^{nd} order autocorrelation function is symmetric around $\tau = 0$ ($A_2(\tau) = A_2(-\tau)$) and therefore it is unable to determine the asymmetry of the pulse temporal shape.
Assuming that the imput intensity has a gaussian shape, the second order autocorrelation function has a gaussian shape too. The relation between the full width at half maximum (FWHM) of the imput intesity τ_p and the FWHM of A_2, τ_{ac} is (see Appendice A):

$$\tau_p = \frac{\tau_{ac}}{\sqrt{2}} \tag{6}$$

On the contrary, the 3^{rd} order autocorrelation function Eq. (4) is an asymmetric function therefore it is suitable to determine the asymmetry of the pulses under study [1] and it presents also a less pronounced smoothing action. The autocorrelation function A_n defined in Eq. (3), for $n > 1$ has the same shape of the pulse represented by intensity profile $I(t)$. In fact, for a resonable peaked function $I(t)$:

$$\lim_{n\to\infty} I^n(t) \propto \delta(t) \tag{11}$$

thus the shape of the autocorrelation signal becomes a trustful approximation of the signal $I(t)$.

[1] The symmetry around $\tau = 0$ for the second order autocorrelation function is shown by:

$$A_2(\tau) = \int_{-\infty}^{\infty} I(t) \cdot I(t-\tau) dt =_{\tau\to-\tau} \int_{-\infty}^{\infty} I(t) \cdot I(t+\tau) dt \tag{7}$$

which, using the relation Eq. (5) shows that

$$A_2(-\tau) = A_2(\tau) \tag{8}$$

while the asymmetry for the third order autocorrelation is shown by

$$A_3(\tau) = \int_{-\infty}^{\infty} I(t) \cdot I^2(t-\tau) dt \tag{9}$$

exchanging: $\tau \to -\tau$

$$A_3(-\tau) = \int_{-\infty}^{\infty} I(t) \cdot I^2(t+\tau) dt =_{t+\tau=y} \int_{-\infty}^{\infty} I(y-\tau) \cdot I^2(y) \tag{10}$$

Eq.(4) shows that if the second term in the integral were a $\delta - function$ the equation would become:

$$\begin{aligned}\lim_{n\to\infty} A_{n+1}(\tau) &= \lim_{n\to\infty}\int_{-\infty}^{\infty} I(t)\cdot I^n(t-\tau)dt \\ &= \int_{-\infty}^{\infty} I(t)\cdot\delta(t-\tau)dt = \int_{-\infty}^{\infty} I(y+\tau)\cdot\delta(y)dy \\ &= I(\tau) \end{aligned} \quad (12)$$

Usually to generate a 2^{nd} autocorrelation the two beams are mixed into a non-linear crystal like a $\beta - Barium - Borate$ (BBO) to produce by a second harmonic generation process (SHG) [10,11,9,7,12], a signal that results to be proportional to the second order autocorrelation function [12]. Changing the optical path of one of the two light beams it is possible to temporally delay the reference beam $I(t-\tau)$.

In the case of the *cross correlation* the two signals are different and we refer to Eq. (1). A cross-correlation process is usually adopted when one of the two signals has a temporal length much shorter than the other so that it can act as a "$\delta - function$". For this process it does no matter the symmetry of the function since the two signals are different. Moreover, the scanning nature of the technique which produces the signal is enough to find out the asymmetry of the pulse under study.

Practically the measure is done by sending the reference pulse (the "$\delta - function$"), which is supposed to have a very short time width with respect to the signals we want to measure, through a controlled optical delay line used to scan the longer pulse profile. For this reason this technique is also called "scanning cross-correlation".

The reason why the technique described above can be based on a nonlinear interaction of the reference pulse and the signal into a non linear crystal for harmonic generation, is that the interaction in the crystal has electronic origin so the nonlinearity is fast enough to measure pulses down to $10^{-14}s$ duration [10]. Unfortunately, because of the UV absorption edge of optical crystals, SHG process can't be used for short wavelength $(\lambda < 380nm)$ [10–12].

As already said before, the measurement of UV pulses is made through Different Frequency Generation (DFG) process, which is a non linear process of the same type of SHG. Both these processes arise from the second order non linearity found in non linear crystals such as $\beta - Barium - Borate$ (BBO).

Since the SHG process like DFG gives a signal proportional to the product of the input intensities [11,12,10] as it is shown by Eqs. (13) and (14), it is possible to show that the intensity of the output signal, as a function of time, it is proportional to the correlation

function (see below).

$$\text{SHG} \qquad I(2\omega, l, t) = \frac{2\omega_1^2 d_{eff} l^2}{n^3 c^3 \varepsilon_0} I(\omega, t) I(\omega, t) [\frac{sin(\triangle kl/2)}{\triangle kl/2}]^2 \tag{13}$$

where in this case: $\omega_2, \omega_3 = \omega$,$\omega_1 = \omega_3 + \omega_2 = 2\omega$ and $\triangle k = k_1 - (k_3 + k_2) = k_{2\omega} - k_\omega$.

$$\text{DFG} \qquad I(\omega_1, l, t) = \frac{2\omega_1^2 d_{eff} l^2}{n_1 n_2 n_3 c^3 \varepsilon_0} I(\omega_3, t) I(\omega_2, t) [\frac{sin(\triangle kl/2)}{\triangle kl/2}]^2 \tag{14}$$

where in this case: $\omega_1 = \omega_3 - \omega_2$ is the different frequency generated from the input frequency $\omega_3 > \omega_2$, l is the crystal length, n_i are the refraction index for the different frequencies, ε_0 is the dielectric constant in vacuum, d_{eff} is the non linear coupling coefficient and $\triangle k = k_1 + k_2 - k_3$. Usually the crystal is cut in order to satisfy the *"phase-matching condition"*: $\triangle k = 0$ by which the maximum efficiency conversion is obtained for the given crystal characteristic. Eqs. (13) and (14), give the intensity of the output beam and if the intensity profile $I_i(t)$ are temporally shifted one respect to the other then the generated electronic signal $S(\tau)$ produced by a photodiode illumminated by the output beam, for the process taken into account, is proportional to the cross-correlation function. In fact, considering the DFG process, expressing the intensity profile as: $I_1(\omega_3, t)$ and $I_2(\omega_2, t - \tau)$ and integrating over time because the detection is made through a photodiode, Eq.(14) becomes:

$$S(\tau) = \frac{2\omega_1^2 d_{eff} l^2}{n_1 n_2 n_3 c^3 \varepsilon_0} \int I_1(\omega_3, t) I_2(\omega_2, t - \tau) dt. \tag{15}$$

Since in our case the $I_2(\omega_2, t - \tau)$ is much shorter in time than $I_1(\omega_3, t)$, it behaves like a $\delta - function$ so the equation yields:

$$S(\tau) = \frac{2\omega_1^2 d_{eff} l^2}{n_1 n_2 n_3 c^3 \varepsilon_0} I_1(\omega_3, \tau) \tag{16}$$

as already explained before.

2 System description

The SPARC laser system (see [4]) is a Ti:Sa laser made up of 4 main parts: the oscillator delivers pulses with central wavelength $\lambda = 800nm$ at a repetition rate $r.r. = 79.9MHz$ with time length of $100fs$ and average power of $800mW$. The pulses enter into a Ti:Sa amplifier based on CPA amplification chain [13] [14]. The amplifier is based on a stretcher that spread out temporally the pulse up to $\sim 200ps$ [15] [16] [17]. Then the pulses are amplified respectively by a regenerative amplifier RGA and a 2-stage multi-pass. Finally

they are re-compressed back to about the initial pulse length. The CPA amplification stage delivers an energy per pulse of $50mJ$ at $r.r. = 10Hz$. After the amplifier the pulses go into a wavelength conversion stage. This is composed by a SHG and a SFG stages both based on type-I BBO crystal. The conversion process is what follows: IR pulses at frequency $\omega_2 = \omega$ are frequency doubled into the SHG crystal producing signal at frequency 2ω. Then the two signals at frequency ω and 2ω are mixed into the SFG crystal to produce a signal at $\omega_3 = 3\omega$; see Fig. (1). This conversion stage delivers UV pulses ($\lambda = 266nm$) with energy up to $\sim 4mJ$.
Then the pulses go into a 2-grating UV stretcher with a variable gratings distance in order to change the time pulse-length. The out-coming pulses have an energy up to $\sim 1.7mJ$ because of the 60% efficiency of each grating.
To measure the UV time pulse length a cross-correlator device based on DFG process is made using a BBO crystal by mixing a part of the IR pulses with the UV pulses; see Fig. (1). As previously discussed and from Eq. (16) the signal produced is proportional to the cross correlation function of the UV pulses of intensity I_1 with the IR pulses of intensity I_2 which is the reference pulse:

$$I(3\omega - \omega, l) = \frac{2(3\omega - \omega)^2 d_{eff} l^2}{n_1 n_2 n_3 c^3 \varepsilon_0} \int I_1(3\omega, t) I_2(\omega, t - \tau) dt. \tag{17}$$

The signal is acquired through a photodiode coupled to the oscilloscope; before the photodiode there is a filter centered at $\lambda = 400nm$ with a bandwidth of $\triangle\lambda = 10nm$. The photodetector used is a high speed silicon model "DET 210" from Thorlabs with a rise and fall time of $1ns$, and a spectral response between $(200 - 1100)nm$. A software has been developed [2] to control the optical delay line length using a stepper motor and to acquire the data from the oscilloscope. The code allow to set the number of point (sampling point) at which the acquisition has to be made and that will reconstruct the UV pulse shape. These points are linked to the pulse space length or time length. The oscilloscope makes a peak-to-peak statistics on the signal obtained and the mean value is acquired from the software as well as the standard deviation. The peak-to-peak statistics is required to eliminate the pulse-to-pulse intensity fluctuation.

3 Resolution of the Correlator

In order to find out what could be the best resolution of the correlator, some measures of the UV pulses as they are coming out from the third harmonic generator without going into the final UV stretcher, are taken. This is the shortest UV pulse that is possible to

[2]We are grateful to: Giampiero di Pirro, Sandro Fioravanti, Federico Anelli from INFN, Laboratori Nazionali di Frascati (LNF), who helped us with the software development.

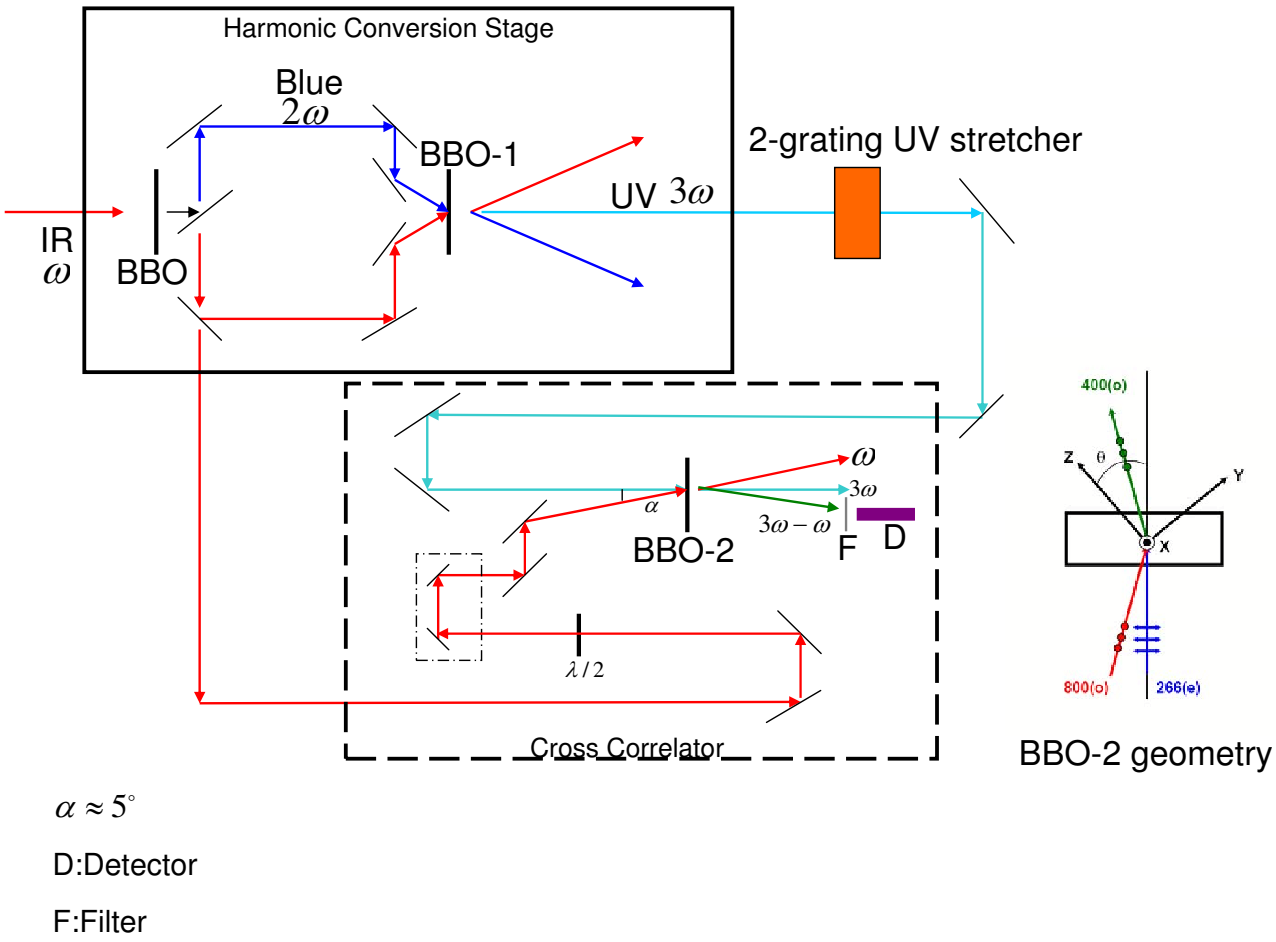

Figure 1: Frequency conversion scheme and the cross correlator of the SPARC laser system. The interaction geometry for the DFG among crystal, incoming and outcoming beams is also shown.

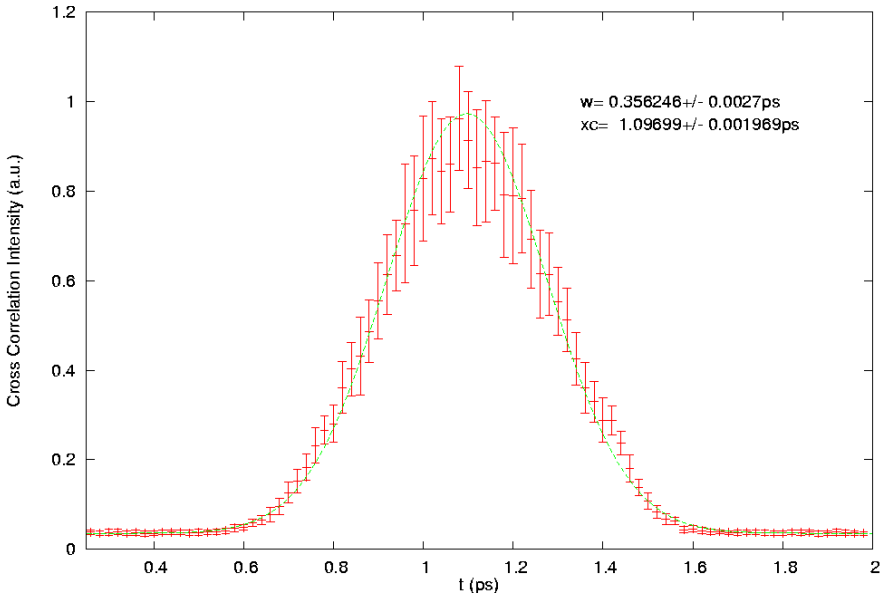

Figure 2: UV autocorrelation signal when the final UV stretcher is bypassed. This data has been used to determine the cross correlator resolution.

achieve in the SPARC laser system and we measured its temporal width also to estimate the resolution of the correlator. In this case the IR signal that in the usual operational mode is the scanning signal, is suppose to have the same temporal shape (gaussian) with the same FWHM.

To seek out the best resolution, the amplifier compressor has been moved varying the positions around what we think to be the best compression point. In Fig. (2) it is shown the shortest pulse shape obtained.

It is important to stress the fact that even though the measured FWHM of the autocorrelation signal is $FWHM \sim 414fs$ which corresponds for Eq (23) (see Appendix A) to a FWHM of the UV signal of about $207fs$, the resolution of the correlator could be even better. In fact, because of the stepper motor range resolution of the compressor, it is not easy to find the exact path lenght inside the compressor itself that the beam has to follow to be re-compressed back around its minimum temporal width (FWHM). The shortest FWHM that the pulses should reach out the compressor is $\sim 150\ fs$.

In all the measures regarding the cross correlation measures, the full width at half maximum (FWHM) has been obtained by fitting the curve with a gaussian shape plus a background. The fit contains four parameters: the background f, the gaussian relative ampli-

tude A, the peak position t_0 and the gaussian size w.

$$G(t) = f + \frac{A}{w \cdot \sqrt{2 \cdot \pi}} \cdot \exp\left[\frac{-2(t-t_0)^2}{w^2}\right] \tag{18}$$

With this definition the FWHM is given by:

$$FWHM = \sqrt{2\ln 2} \cdot W = 1.177 \cdot w \tag{19}$$

In the fitting process, only the points which represents the principal bell shape of the curves have been considered ignoring the possible lateral modulations.

4 Spatial chirp effects

In the initial configuration of the SPARC laser system, the final UV stretching is performed by sending the beam in a single pass 2-grating UV stretcher ($4350 grooves/mm$ each grating) as it is shown in Fig (1) where the stretcher is drawn as a black box. The input beam is spatially dispersed by the first grating and then recollimate through the second. Different wavelengths travel different optical paths so the pulse broadens temporally. The stretching factor is dependent on the input pulse bandwidth and proportional to the gratings distance that can be easily adjusted to obtain pulses length ranging between $600fs$ to $12ps$. The output beam thus experiences a spatial chirp due to the single pass configuration.
In other words along the transverse direction to the beam, which on the following we refer to as $x - direction$, there is a variation of the frequency distribution as it is shown in Fig. (3). In order to describe this effect, it is possible to define locally a spectral amplitude modulation obtained by all the intensity contributions that each frequency component assumes in that specific point. So the resulting spectrum at that point can be represented by the total spectrum times an amplitude modulation in such a way Eq. (20)

$$S_{local}(\lambda, x) = S_{tot}(\lambda) \cdot A(\lambda, x) \tag{20}$$

where: $S_{local}(\lambda, x)$ is the local resulting spectrum, $S_{tot}(\lambda)$ is the total spectrum of the laser beam and $A(\lambda, x)$ is the spectral amplitude modulation. The spectral amplitude modulation has been obtained by adopting the following model: it has been assumed that each frequency component has a gaussian form with the FWHM equal to the beam waist $\triangle x$:

$$G(l, \delta\lambda, \triangle x, x) \propto \exp\left[\frac{-2(1.177)^2}{(\triangle x)^2}\left(x - \triangle(l, \delta\lambda)\right)^2\right] \tag{21}$$

where $\triangle(l, \delta\lambda)$ takes into account the displacement of the gaussian peak as a function of λ introduced by the grating with respect to x_0 which is the central position of the outcoming

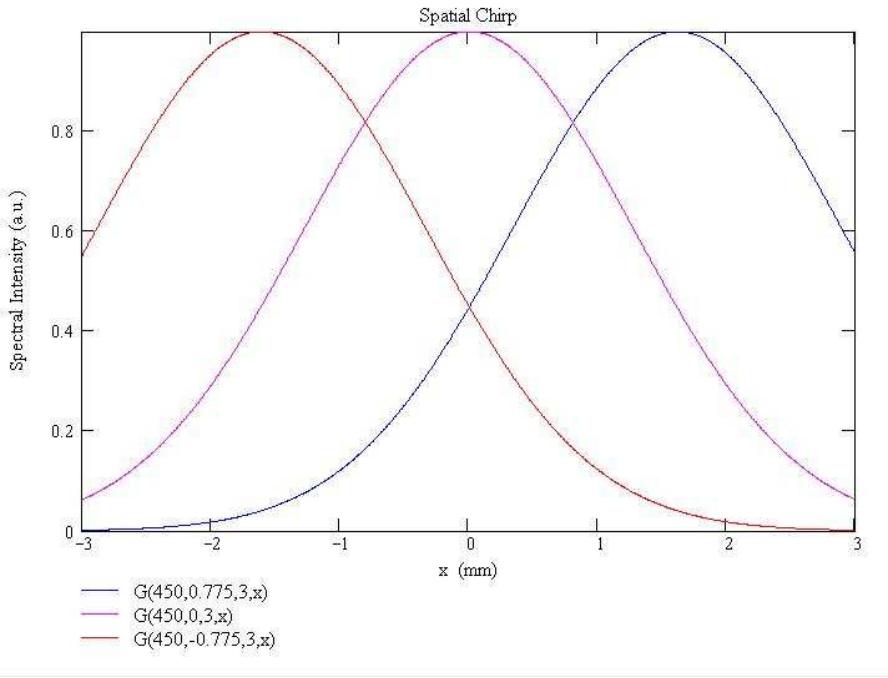

Figure 3: The picture shows the spatial chirp effect: a frequency components distibution along the UV transverse direction x according to the definition of $G(l, \delta\lambda, \triangle x, x)$

beam corresponding to the central wavelength λ_0. The displacement $\triangle(l, \delta\lambda)$ depends on the path followed by the beam between the two gratings l, on the variation $\delta\lambda$ respect to λ_0 and on the angle of the incoming beam respect to the first grating.
In Fig (3) we show the frequency modulation for three different λ values as a function of the transverse positions respect to x_0. Thus the amplitude modulation $A(\lambda, xl, \delta\lambda, \triangle x, x)$ shown in Fig (4) is obtained by keeping fixed in Eq. (21) the $x - variable$ and varying the $\delta\lambda - variable$.
The spatial chirp can affect the cross correlation measures by two different effects that will be discussed below.

4.1 Alignment effects

In the cross correlator, all the frequency components of the IR beam that is not spatially chirped and acts as scanning signal, will interact through the crystal overlapping region with the modulated spectrum Eq.(20), for that region, of the UV beam. Thus a small change of the angle α (UV line is fixed; see Fig. (1) between the IR beam and the UV beam, will modify the interaction region of the IR beam along the UV beam, changing

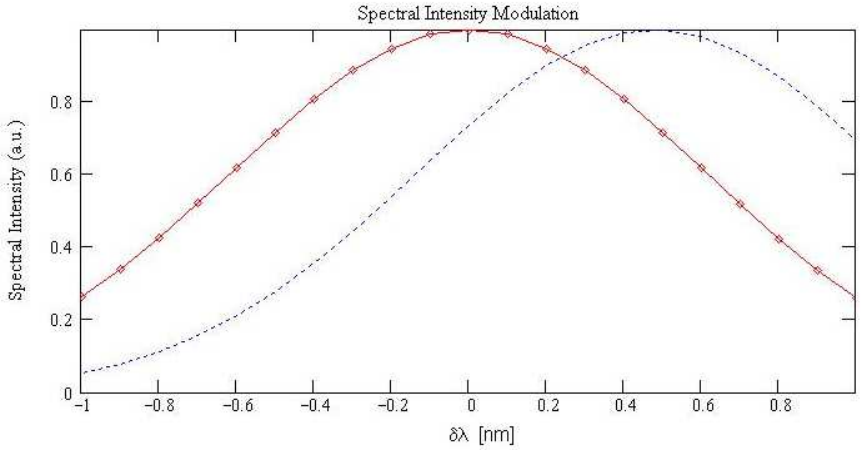

Figure 4: The picture shows two different spectral intensity modulations obtained for a misalignment of $x = 1mm$

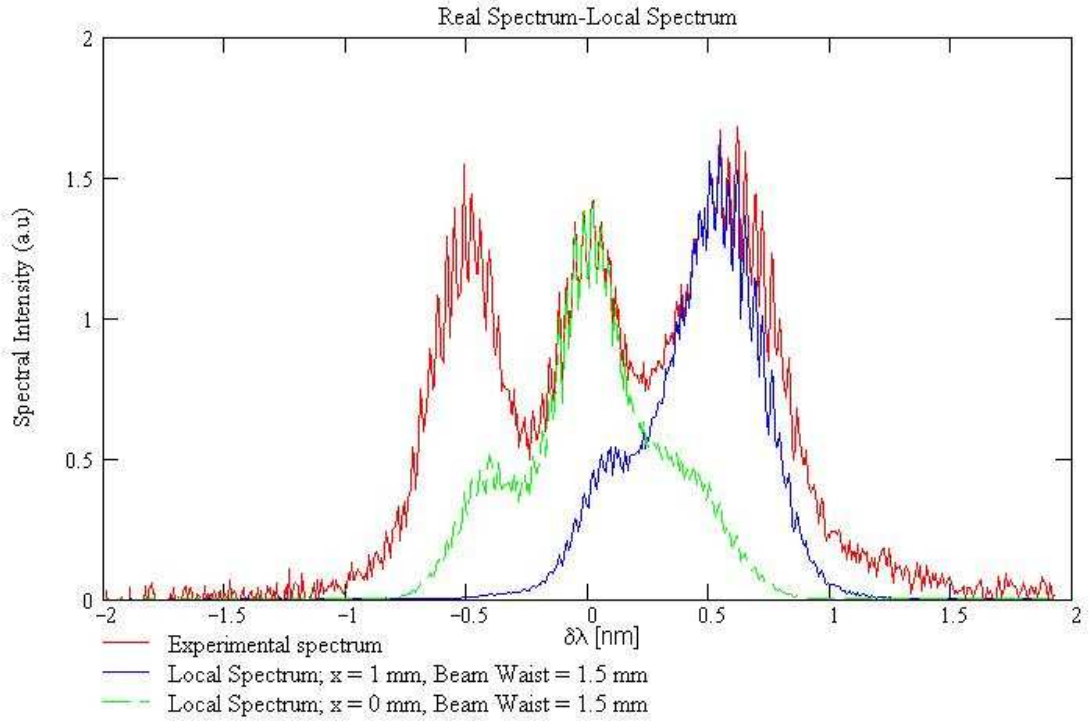

Figure 5: Red line: experimental spectrum; green and blu line: simulation showing the effect of the spatial chirp on the alignment; the difference between green and blu line is a misalignment of $x = 1mm$. In the figure are also reported the values used in Eq. (21) to calculate $A(\lambda, x)$

the spectral modulation function. This meccanism causes a sensitive changing in the spectrum of the outgoing pulse which is going to be detected.

In Fig. (5) it is possible to see how it would be the local UV spectrum (blue and green line) when two different spectral amplitude modulations are applied on the experimental total spectrum (red line). The modulations are obtained by changing the angle between the two beams. In Fig. (5) it is clearly shown that the two resulting spectra (blu and green line) have a different bandwidth compare to each other and to the total spectrum (red line). It is also shown that the spectrum shapes have a different profile.

In Fig.(6), (7) are shown two cross correlation measures for two different input angle between the UV and IR beam. The two figures reveal a different time width as a result of the different bandwidth due to the misalignments.

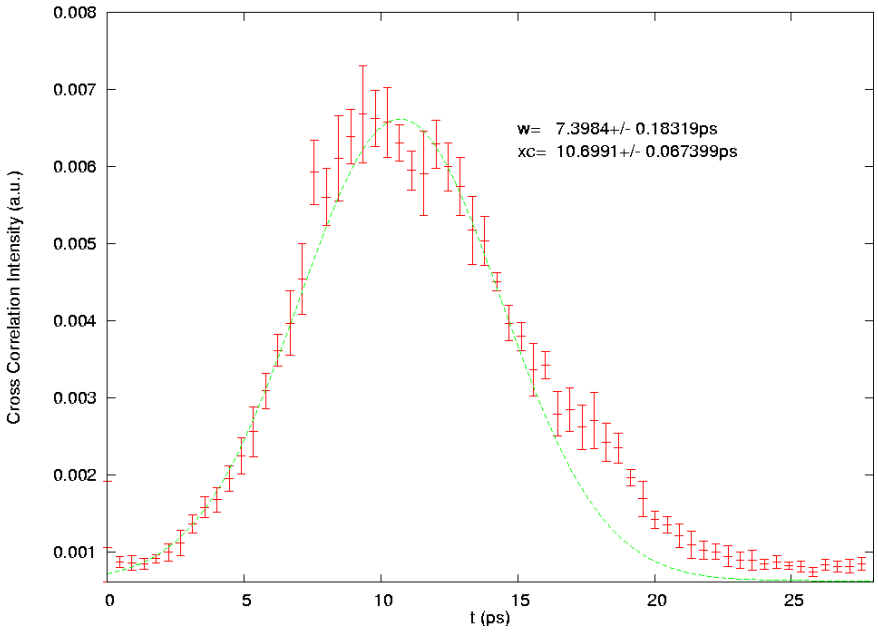

Figure 6: Almost complete spatial overlapping between UV and IR spot

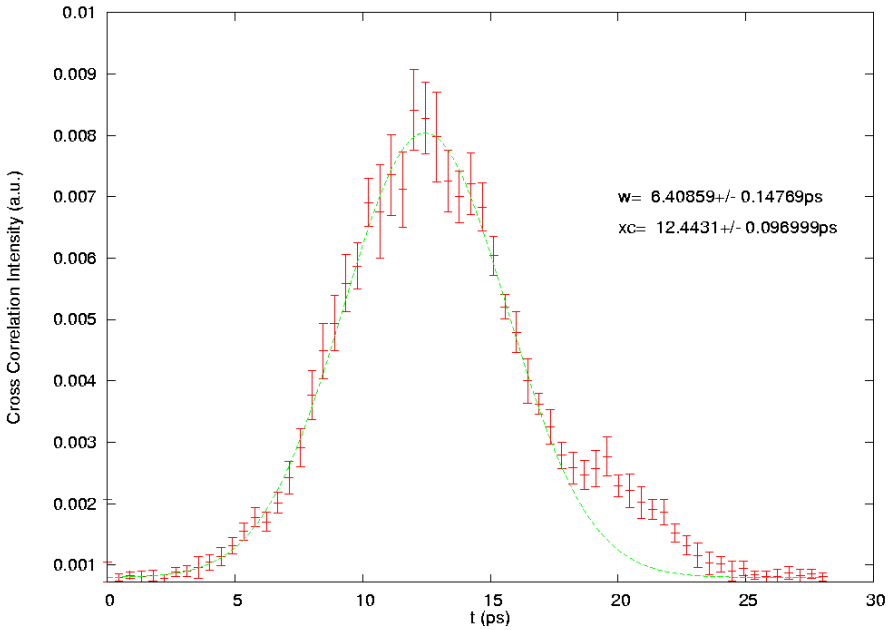

Figure 7: Non complete spatial overlapping between UV and IR spot since the angle has been changed

4.2 Spot size dependence

The presence of the spatial chirp makes pulse width and the cross correlation measures to be dependent on the beam spot size. In fact every time the beam spot is cut, there is a loss in the spectral bandwidth of the beam, therefore the cross correlator gives the measure of the temporal profile for the beam with a reduced frequency components; and consequently a different pulse width is measured.
In order to study this effect, several measures have been taken changing the beam spot size by an iris and keeping the angle between the UV and the IR beam fixed. The results are shown in Fig. (8) and Fig. (9) where it is possible to see that the FWHM of the two different profiles differs about $1.5ps$. For this reason every time the beam spot clips there is a filtering process of the frequency components. Note that the two shapes in time are not completely gaussian but there is a shoulder to the right that is out of the fit. Looking at Fig (5) where we have shown the results of the spatial chirp model, we observe an effect very similar in the spectrum shape and therefore we believe that it is a side effect of the spatial chirp.

4.3 Spectrum reported in time

It has been shown [18] that, when the temporal chirp is large enough, the spectral intensity profile of the pulse is reproduced in time (This means that under this conditions the cross correlation measure should be very similar to the spectral intensity profile). Unfortunately this phenomena can not be seen because of the spatial chirp. In fact as explained before, changes in the beam spot size, modify the spectrum giving rise also to a reduction of the temporal chirp introduced by the grating stretcher. Therefore the condition required for this phenomena is not satisfied in our set-up.

5 Conclusion

In this paper it has been reported the physics behind the cross correlation technique and some measurements are shown. The resolution of the cross correlator built for the SPARC project has been found out to be $< 360fs$; it is much better than a high resolution streak camera which is also expensive more than one order of magnitude with respect to the cross correlator.
It has been discussed how the presence of the spatial chirp, due to the final UV single pass stretcher, affects the measurements by changing the characteristics, the bandwidth and the shape, of the outgoing pulse that is detected.
In conclusion, it is extremely important for the cross correlation technique to give exact

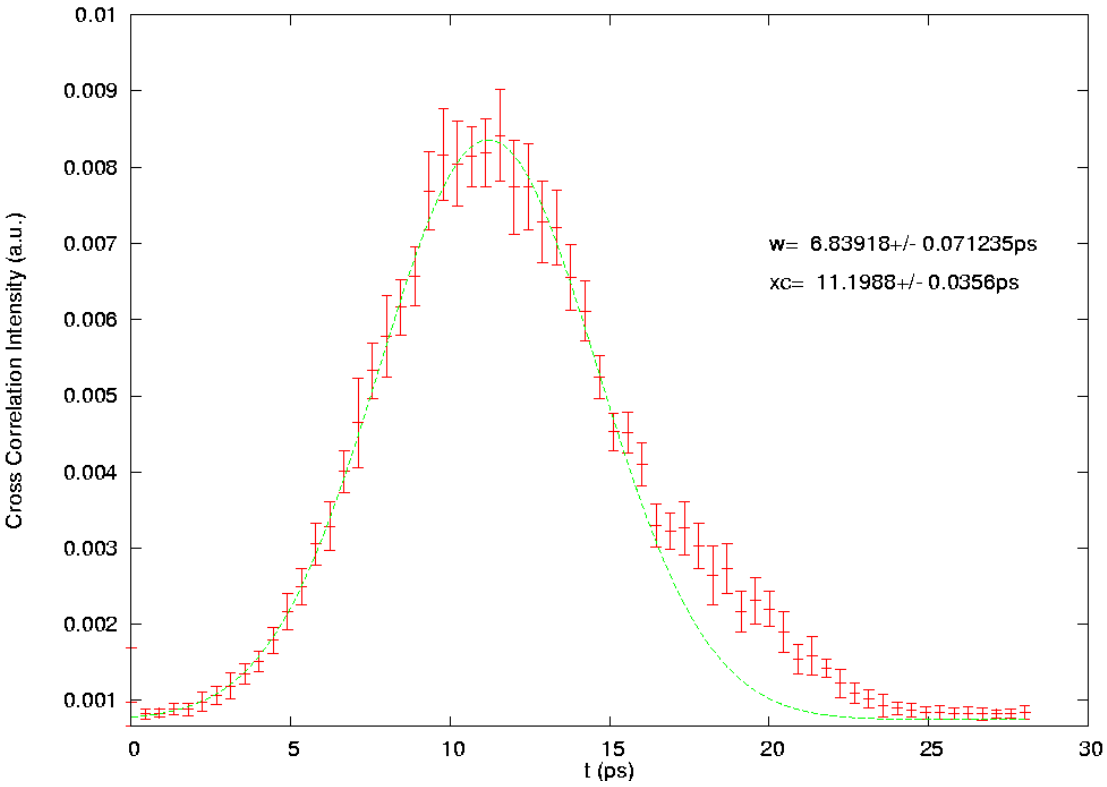

Figure 8: Beam spot size effect: all the UV beam spot enters the crystal

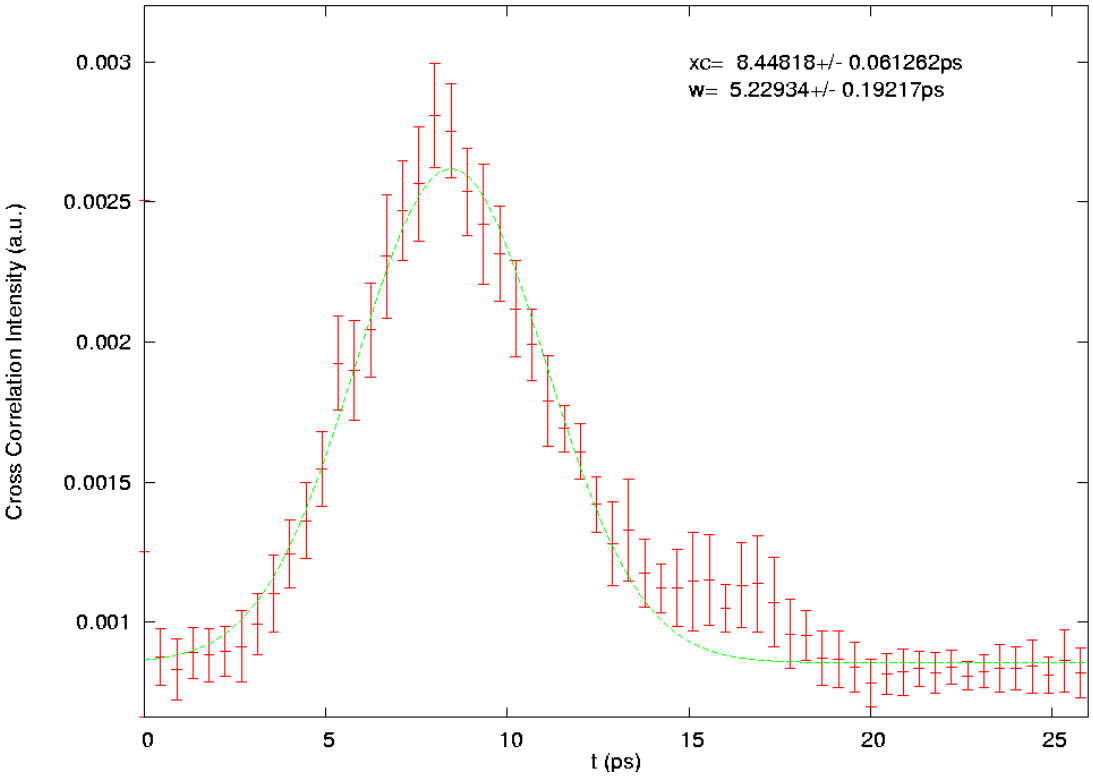

Figure 9: Beam spot size effect:a part of the UV beam spot is cut by an iris

informations about the entire pulse under study. To avoid the presence of the spatial chirp in the UV beam a modification of the UV stretcher is foreseen

6 Appendix A

In the common application the autocorrelation trace is a SHG signal obtained by mixing two beam coming from the same laser beam previously splitted. Being the SHG signal proportional to the intensity product of the two beam (13), the pulse length τ_{ac} of the autocorrelation signal is related to the pulse length τ_i of the initial pulses in this way:

$$\tau_i = \frac{\tau_{ac}}{\sqrt{2}} \tag{22}$$

where it has been assumed a gaussian shape for the initial laser pulses.
In our case, always assuming a gaussian shape for the initial IR laser pulses $I_{IR}(t)$, we find out that the relation between the pulse length of the autocorrelation signal with the pulse length of the UV pulses obtained by converting the initial IR pulses by a third harmonic generation process is:

$$\tau_i = \frac{\tau_{ac}}{2} \tag{23}$$

This can be shown as follow:
assuming:

$$I_{IR}(t) \propto \exp[-2 \cdot (\frac{t}{\tau_i})^2] \tag{24}$$

we have that the UV intensity shape is:

$$I_{UV}(t) \propto \exp[-3 \cdot 2 \cdot (\frac{t}{\tau_i})^2] = \exp[-2 \cdot (\frac{t}{\tau_{uv}})^2] \tag{25}$$

where $\tau_{uv}^2 = \tau_i^2/3$ is the UV pulse length, in fact the UV signal is proportional to the intensity product of the IR beam and the blue beam generated by the SHG process which is itself equal to the IR intensity product of the two beam striking the first BBO crystal, thus $I_{UV} = I_{IR}^3$. The cross correlation signal is Eq. (16):

$$I_{ac}(t) \int_{-\infty}^{\infty} I_{UV}(t) \cdot I_{IR}(t-\tau)dt = \int_{-\infty}^{\infty} I_{IR}(t)^3 \cdot I_{IR}(t-\tau)dt \tag{26}$$

thus it results to be

$$I_{ac}(t) \propto \exp[-2 \cdot (\frac{t}{\tau_{ac}})^2] \tag{27}$$

where $\tau_{ac} = \frac{2}{\sqrt{3}} \cdot \tau_i = 2\tau_{uv}$. Using this relation it is possible to retrive the UV temporal pulse length τ_{uv} by the measured cross correlation pulse width τ_{ac}. It follows that for a UV gaussian pulse, that is the third harmonic signal of a gaussian IR pulse, the cross correlation yields a results which is twice the effective pulse length of the UV.

References

[1] Editori: L. Palumbo, J. Rosenzweig. Autori: D. Alesini et al. (INFN/LNF), F. Alessandria et al. (INFN/Milano), D. Levi, M. Mattioli, G. Medici (INFN/Roma1), L. Catani et al. (INFN/Roma2), G. Dattoli et al. (ENEA/FIS), S. Reiche, J. Rosenzweig, G. Travish (UCLA), D. Dowell et al. (SLAC), *Technical Design Report for the SPARC Advanced Photo-Injector*, Preprint INFN National Laboratories of Frascati, 12/01/2004

[2] SPARC *Conceptual design of a high-brightness linac for soft X-ray SASE-FEL source*, Proceedings of EPAC 2002 (La Villette, Paris), 5 June 2002

[3] C. Vicario, M. Petrarca, A. Ghigo, *Laser temporal pulse shaping experiment for SPARC photoinjector*, Proceedings of EPAC 2004 (Lucerne, Switzerland)

[4] C. Vicario et al., *Plans for the Laser System for the SPARC test photoinjector*, in Physics of High Brightness Beams, (World Scientific, Singapore, 2003).

[5] M. Reiser, *Theory and Design of Charge Particle Beams*, (Wiley & Sons, Inch, N. Y., 1994)

[6] C. A. Brau, *What Brightness Means*, in Physics of High Brightness Beams, (World Scientific, Singapore, 2003)

[7] J. C. Diels, W. Rudolph, *Ultrashort Laser Pulse Phenomena*, (Optics and Photonics, Accademica Press Inch, N. Y., 1996).

[8] A. E. Siegman, *Lasers*, (University Science Books, Sausalito, California, 1986)

[9] O. Svelto, *Principles of Laser*, (Plenum Press, New York, 1998).

[10] Boyd, *Nonlinear Optics*, (Academic Press)

[11] A. Yariv, *Quantum Electronics*, (Wiley, New York, 1989, 3rd ed.).

[12] E. P. Ippen, *Nonlinear Optics*, **6.635**, Spring

[13] P. Maine, D. Strickland, P. Bado, M. Pessot, G. Mourou, *IEEE J. Quantum Electronics* , **24**, 398, (1988).

[14] S. Backus, Charles G. Durfee III, Margaret M. Murnane, Henry C. Kapteyn, *High power ultrafast lasers*, Review of Scientific Instruments, **69** no. 3, 1207, (1998).

[15] O. E. Martinez, J. Opt. Soc. Am. B **3**, 929, (1986).

[16] E. B. Treacy, *IEEE J. Quantum Electronics* , **QE-5**, 454, (1969).

[17] O. E. Martinez, *IEEE J. Quantum Electronics* , **23**, 59, (1987).

[18] S. Cialdi, I. Boscolo *A shaper for providing long laser waveforms*, **INFN/BE-04-01**, 06-02-2004